This is a repository copy of *The role of surface pre-treatment on the microstructure, corrosion and fretting corrosion of cemented femoral stems*.

White Rose Research Online URL for this paper:
http://eprints.whiterose.ac.uk/95388/

Version: Accepted Version

Article:

Bryant, M, Farrar, R, Freeman, R et al. (2 more authors) (2016) The role of surface pre-treatment on the microstructure, corrosion and fretting corrosion of cemented femoral stems. Biotribology, 5. pp. 1-15. ISSN 2352-5738

https://doi.org/10.1016/j.biotri.2015.12.001

The Role of Surface Pre-treatment on the Microstructure, Corrosion and Fretting Corrosion of Cemented Femoral stems

M.Bryant*[a], R. Farrar[b], R. Freeman[b], K. Brummitt[b], A. Neville[a]

a - Institute of Functional Surfaces (iFS), School of Mechanical Engineering, University of Leeds, UK**.**

b- DePuy Synthes, Leeds, United Kingdom

M.g.bryant@leeds.ac.uk

(+44) 113 343 2161

Abstract

The use of cemented femoral stems is common practice worldwide with strong clinical data supporting their use. Over the years, different surface processing techniques have been employed to enhance the performance of the stem-cement interface. As a result different clinical outcomes and visual presentation at revision has been observed. Whilst research has focussed on increasing adhesion and better load bearing capacity, the effects of surface processing on the degradation of cemented femoral stems has not been investigated. The aims of this study was to investigate the effects of surface processing on the subsurface microstructure, surface chemistry and tribocorrosion degradation mechanisms of cemented tapered femoral stems subjected to polishing and blasting (Vaquasheen) processes. Cemented femoral stems were orientated and loaded according to ISO 7206-4 for 500,000 cycles in 0.9% NaCl at 37 ˚C. A three-electrode electrochemical cell was integrated into the mechanical test to facilitate in-situ corrosion measurements. The severity and mechanism of damaged were assessed scanning and transmission electron microscopy, X-ray photoelectron spectrometry, solution mass spectrometry and white light interferometry. Surface processing was seen to drastically influence the level of corrosion within the interface with polished surfaces demonstrating the highest levels of corrosion. Surface analysis consistently demonstrated the presence of a SiO_2 layer on the vaquasheened stems thought to originate from the glass bead blast matrix. This resulted in lower levels of corrosion both under static and tribocorrosion assessment. In conclusion, blasted surfaces resulted in lower wear induced corrosion when compared to the polished surfaces. However the total metallic ion levels did not follow the same trend. This is thought to be due to the formation of metallic debris and dissolution of debris due to abrasion of the femoral stems.

Keywords: Fretting-corrosion, bone cement, surface roughness, CoCr alloy, surface analysis, electrochemistry

The Role of Surface Pre-treatment on the Microstructure, Corrosion and Fretting Corrosion of Cemented Femoral stems

Abstract

The use of cemented femoral stems is common practice worldwide with strong clinical data supporting their use. Over the years, different surface processing techniques have been employed to enhance the performance of the stem-cement interface. As a result different clinical outcomes and visual presentation at revision has been observed. Whilst research has focussed on increasing adhesion and better load bearing capacity, the effects of surface processing on the degradation of cemented femoral stems has not been investigated. The aims of this study was to investigate the effects of surface processing on the subsurface microstructure, surface chemistry and tribocorrosion degradation mechanisms of cemented tapered femoral stems subjected to polishing and blasting (Vaquasheen) processes. Cemented femoral stems were orientated and loaded according to ISO 7206-4 for 500,000 cycles in 0.9% NaCl at 37 ˚C. A three-electrode electrochemical cell was integrated into the mechanical test to facilitate in-situ corrosion measurements. The severity and mechanism of damaged were assessed scanning and transmission electron microscopy, X-ray photoelectron spectrometry, solution mass spectrometry and white light interferometry. Surface processing was seen to drastically influence the level of corrosion within the interface with polished surfaces demonstrating the highest levels of corrosion. Surface analysis consistently demonstrated the presence of a SiO_2 layer on the vaquasheened stems. This resulted in lower levels of corrosion both under static and tribocorrosion assessment. In conclusion, blasted surfaces resulted in lower wear induced corrosion when compared to the polished surfaces. However the total metallic ion levels did not follow the same trend. This is thought to be due to the formation of metallic debris and dissolution of debris due to abrasion of the femoral stems.

1. Introduction

Recent research has shown that a combination of wear and corrosion at the stem-cement interface results in the generation of metallic ions and polymer debris along with damage of the femoral stem, counterpart PMMA bone cement and ultimately failure due to soft tissue reactions [1-3]. A considerable amount of work has also been performed to improve the interfacial bond between the stem and the cement mantle. Cementing techniques, surface roughness patches, textures and pre-coatings have all been considered in order to achieve reliable

2

fixation according to Webb et al [4]. The wear and corrosion at the stem-cement interface isn't a recent observation. Willert et al [5] presented evidence of crevice corrosion of twenty eight cemented titanium alloy Müller straight femoral stems complimented by analysis of the pH of the fluids trapped within the interface. A decrease in the pH indicated that crevice corrosion was evident; exacerbated by a 'pumping' action of the fluid about the interface caused by mechanical loading. It was concluded that that the mechanism of crevice corrosion for these cemented titanium based alloys was not applicable to cobalt and iron based implant alloys.

Depending upon the design philosophy of the femoral stem, different surface finishes have been adopted [6]. For taper loaded femoral stems, such as the Exeter™ (Stryker, USA), CPT™ (Zimmer, USA), C-Stem™ and Ultima TPS™ (DePuy Synthes, UK), a highly polished surface finish is desired. This aids controlled migration and slip of the femoral stem with the minimum generation of debris. An increased surface roughness is generally chosen for composite beam stems to increase interfacial strength and to reduce instances of slip or migration at the interface. It is generally well accepted for these designs to be successful, the bond between the femoral stem and PMMA bone cement must be maintained for long term stability. This is supported by historical evidence of the 'matte' Exeter femoral stems (taper loaded geometry). These were considered unsuccessful due to high incidences of PMMA induced inflammatory reactions due to abrasion at the interface [6]. Whilst all femoral components display some form of wear and corrosion at revision, the different interfacial conditions produce very different surface morphologies as demonstrated by Howell et al [7]. They noted that blasted femoral stems tend to demonstrate light polishing on the medial and lateral edges, whilst polished femoral stems demonstrate high incidences of fretting related damage.

It is only of late that the tribocorrosion degradation, described as material loss owing to mechanical and electrochemical reactions, and the factors influencing this have been considered for cemented devices [8-12]. Recently, fretting-crevice corrosion of polished femoral stems has been implicated in the early failure and high revision rates of taper polished femoral stems [13,1,3]. The occurrence of pain and evidence of metal hypersensitivity have been observed in these cases. Although the wear mechanisms acting at the stem-cement interface are fairly well accepted, they tend to be lesser known and assumed when compared to bearing or taper interfaces. Currently only a few studies exist investigating the role of fretting-corrosion and the influence of system variables at the stem-cement interface [8,14,11,15]. Recently the authors have presented systematic work outlining the tribocorrosion mechanisms [15,13] and role of system variables such as cement type [16,17] and mixed metal couples [18] on the overall degradation of cemented femoral stems. This study goes further to

examine the influence of surface processing on the fretting-corrosion characteristics, subsurface microstructure and surface chemistry of cemented femoral stems through the use of in-vitro tribocorrosion simulations and advanced surface analysis techniques.

2.   Materials and Methods

2.1. Experimental Materials, Surface Processing and Preparation

All experiments were conducted on fully cemented LC (low carbon) CoCrMo Ultima TPS™ (DePuy Synthes, Leeds, United Kingdom) femoral stems (Table 1). Each femoral stem was forged from wrought alloy, any excess material removed, stem-taper machined and then the remaining portions (including the cemented portions) polished by Symmetry Medical (Sheffield, UK). Each femoral stem was then inspected for any signs of imperfections, cleaned and packaged by DePuy Synthes.

Table 1 Chemical composition of the Ultima TPS femoral stems tested in this study as stated by manufacturer.

In order to replicate the polishing process femoral implants undergo, each sample was polished using a rotating cloth mop and wax to a 'super finished' surface. To roughen the stems, Ultima TPS™ femoral stem were subjected to a process known as vaqua-sheen; a blasting process involving water and glass beads. This will be referred to as the 'blasted' surface in the study. The beads had the following composition (Table 2). It is important to note that all stems tested in this study were from the same forging batch and subjected to the same thermal processes. All test pieces were cleaned, degreased and then passivated as per manufacturer's specifications. In all tests CMW MV (DePuy Synthes, Blackpool, UK) PMMA bone cement was utilised and prepared according to manufacturer's instructions

Table 2 Composition of bead blasting material used in this study.

The solution used for all electrochemical measurements was aerated 0.9% NaCl solution (pH $\approx$ 7.4) at 37 ˚C, prepared using analytical grade reagents and deionised water. This was to simplify the system, removing the metal-protein interface which has recently been shown to influence the rates of corrosion [19]. Throughout this study a three electrode electrochemical cell consisting of a working electrode (WE), in this case the femoral CoCr stem, Ag/AgCl reference electrode (RE) and Pt counter electrode (CE) (Thermo-Scientific, UK).

2.2. Static corrosion measurements

Potentiodynamic corrosion measurements were conducted using an Autolab PGSTAT101 (Metrohm, Netherlands) to quantify the corrosion characteristics of the femoral stems in the absence of cyclic loading. In order to assess the corrosion properties of the different femoral stems, a flat electrochemical cell was adopted. This enabled 1 cm^2 area of each femoral stem to be exposed to the electrolyte without the need for sample mounting etc. Each sample was immersed in the tests electrolyte at 37˚C and the E_{corr} allowed settle for 1hr prior to polarisation. Potentiodynamic polarisation was then conducted from -100mV vs E_{corrr} and scanned in the anodic direction at a rate of 0.25 mV/sec. At 500 µA/cm^2 the current was reserved and the scan terminated when the current had reached the resolution of the instrument. Full details of the protocol can be found at [17].

2.3. Fretting-crevice corrosion test arrangement

To evaluate the mechanically enhanced corrosion mechanisms at the stem-cement interfaces a tribocorrosion test apparatus and procedure was develop and conducted in part reference to ISO 7206-4. Full details of the experimental arrangement and electrochemical method have been reported elsewhere [16,15]. In brief, cemented femoral stems were orientated at 9 and 10˚ flexion and extension, respectively, and subjected to a compressive sinusoidal load (0.3-2.3 kN) at 1 Hz. A 3 electrode electrochemical cell was incorporated into the cell to facilitate in-situ and real time corrosion rate measurements. These consisted of free corrosion potential and corrosion current determined through linear resistance polarisation (LPR) assuming a Stern-Geary coefficient of 0.026. Corrosion currents were then integrated with respect to time to yield the total charge passed and converted to a corrosive mass loss (i.e. material lost from the interface due to corrosion) using Faradays equation using constants given in [16,15].

Inductively Coupled-Mass Spectrometry (ICP-MS) was used to analyse elemental composition of the electrolytes post-test. 1 mL of test electrolyte was diluted to 10mL with HNO_3 prior to analysis. No effort was made to extract particulate from the electrolyte and so ionic mass measurements represent a combination of ions and particles present in the solution.

2.4. Surface Analysis

To characterise the surface morphology, surface topography, sub-surface morphology and surface chemistry, pre and post testing, a variety of techniques were adopted. Scanning Electron Microscopy (SEM) analysis was conducted using a Carl Zeiss EVO MA15 equipped with Energy Disperse X-ray Spectroscopy (EDX) to facilitate elemental analysis. Imaging was conducted at 20 kV and 5kV in order to investigate interfacial

5

compositions. Focused Ion Beam (FIB) sample preparation and subsequent Transmission Electron Microscopy (TEM) was also utilised as a technique to quantify the exact composition, thickness and morphology of any deposit or corrosion product at a nano-meter scale. Details of the FIB/TEM preparation method are presented in [20].

The crystalline structure of materials was characterised by X-ray diffraction on both samples that had undergone surface pre-treatment. 2θ scans between 40° and 50°were carried out using Cu Kα radiation (X'Pert[3], Phillips, USA) . The scan range selected allows to determine unambiguously the coexistence of the FCC and HCP cobalt phases; within this region the strong $(200)^{fcc}$ and the $(10\bar{1}1)^{hcp}$ are well isolated and do not overlap with any other diffraction peak [21]. A change in peak position and broadening of peaks was observed an indication to the level of strain present within the surfaces.

Surface morphology and textural parameters were analysed by White Light Interferometry (WLI) using a TalySurf CCI (Taylor-Hobson, UK) in order to get a quantitative topographical representation the femoral surface before and after testing. A variety of surface parameters were obtained from the data using Talymap Gold software (Taylor-Hobson, Leicester, UK). A description of parameters used in this study is given in Table 3. All WLI data was fitting to a least square plane and subject to form correction. To obtain spatial surface values, data was passed through a Gaussian filter with a cut-off of 0.08 mm. The real surface area of the surfaces was calculated using algorithms provided by the software. This was used to correct electrochemical polarisation data.

Table 3 Surface morphology parameters (22).

X-ray Photoelectron Spectroscopy (XPS) was further utilised to establish the exact chemical composition of the surface. XPS analysis was carried out using a VG Escalab 250 with a high intensity monochromatic Al Kα X-ray source (1486.6 eV) with a lateral resolution of 500 µm. XPS surveys were initially conducted, followed by high resolution XPS scans on the elements found on the surface. Although X-rays penetrate to a depth of several micrometres, ejected photoelectrons generally come from only the first several nanometres of material making the analysis of the passive film and bulk substrate possible. In order to assess the variation in composition and to mitigate any contamination effects each sample was subjected to an argon-ion etch at $1\mu A/3mm^2$. Using CasaXPS fitting software, the height, area and position of the peaks was determined allowing the separation of measured XPS spectra. The binding energy scale was calibrated for the C1s peak at 284.5 eV. All the results in

this paper use the standard format and units (CPS versus BE). Values of binding energies, FWHM and relative sensitivity factors were taken from literature [22-24].

A Mitutoyo-MVK-Ha micro-hardness testing machine was used to measure materials micro hardness. A load of 110 g was applied and held for 15 secs. Tests were carried out a minimum of 6 times on each area of interest. Nano-indentation was also conducted using a Micro-Materials platform in order to quantify any change in hardness in the top hundreds of nm of the metallic surface due to re-orientation of the crystalline structure of the alloy. Nano-hardness was determined using an incremental load controlled process using a Berkovich diamond indenter. A load controlled method was adopted 100 mN (max depth = 500 nm) and the hardness determined automatically by the apparatus using the Oliver and Pharr method. It is appreciated by the authors that the hardness measurements presented do not fully quantify the nano-mechanical properties of the strain transformed subsurface or any films formed on the surface due to the analysis depth being > 10% of the area of interest. Due to the nature of the surfaces it was not possible to obtain meaningful analysis at such scale. Nevertheless the results obtained and presented demonstrate the role surface processing plays on the nano-mechanical properties of the surfaces and is further supported with XRD and TEM analysis.

In each measurement case, the results presented demonstrate measurement mean (n=3 unless otherwise stated) ± experimental deviation.

3. Results

3.1. Characterisation of Surface Morphology, Topography, Subsurface Morphology and Corrosion Behaviour Prior to Testing

3.1.1. Surface Topography and Crevice Interface

Figure 1 shows the 3D surface topography scans of the polished (Figure 1a) and blasted (Figure 1b) surfaces. A description of each parameter is given in Table 3. For polished femoral stems $S_a = 0.008\pm0.003$ µm, $S_{sk} = -0.31\pm0.23$ and $S_z = 0.26\pm0.21$ µm. The blasting process resulted in an $S_a = 0.51\pm0.01$ µm, $S_{sk} = -0.43\pm0.24$ and $S_z = 7.11\pm0.71$ µm. The surface area for each samples were also calculated for each surface. The real surface area due to topography changes of polished and blasted surfaces was measured as $0.24mm^2/231mm^2$ and $0.28mm^2/240mm^2$ (surface area/area scanned) respectively. These results represent the surface area of the surface per area studied.

Fig 1 Surface Topography after a) polishing and b) blasting processes.

Figure 2 shows Secondary Electron (SE) SEM images of both metallic surface prior to tribocorrosion testing. Polished surfaces (Figure 2a) demonstrated little variations in topography when compared to the blasted surfaces (Figure 2b). SEM and EDX analysis was conducted at lower electron acceleration voltages (5 kV) to reduce the volume fraction of surface analysed (depth ≈150 nm). SEM/EDX analysis and mapping at 5kV demonstrated that surfaces of the polished stems were rich in Co, Cr, Mo, O and C (Figure 3a). Figure 3b presents the EDX mapping for the blasted sample. In addition to the Co, Cr, Mo and O observed on the polished surfaces Si, Ca, S and Mg were also observed on the blasted surfaces. In both cases, elemental abundance seemed evenly distributed across the surfaces.

Fig 2 SE SEM images of a) polished and b) blasted femoral stem prior to tribocorrosion testing

Fig 3 Quantitative EDX mapping of a a) polished CoCr femoral stem in the area presented in Figure 3a and b) a blasted CoCr in the region of interest in Figure 3b.

Figure 4 shows the sections of the interface after the bone cement had cured. Sections prepared using a diamond tipped sectioning saw (Buehler, USA) and metallographic preparation techniques. Differences were noticed depending on the surface roughness of the metallic sample. Interdigitation of the bone cement with metallic surface was seen on the samples that had undergone the aqueous bead blasting process.

Figure 4 Secondary Electron SEM images of the stem-cement interface for a (a) Polished (b) Blasted femoral stem. From cross-sectional analysis of the interfaces the crevice height was seen to be similar in both cases ranging from 2-4 μm.

3.1.2. Micro and Nano-Hardness

Figure 5 shows the micro and nano-hardness values obtained. On average, micro-hardness results demonstrated differences between the polished and blasted surfaces however were not seen to be significant (Figure 5a).

Nano-hardness measurements indicated an increase in hardness within the top 500 nm of both surfaces when compared to micro hardness measurements (Figure 5b). This was seen to increase from 5.07-7.74 and 5.70-7.10 GPa for the polished and blasted surfaces respectively. Whilst an increase in hardness was observed at the different length scales no significant difference was observed between the processing methods. This large variation in measurement is due to the in-homogeneous nature of the blasted surface.

Fig 5 a) Micro hardness of wrought and forged LC CoCrMo and b) Nano-hardness of forged LC CoCrMo when subjected to mechanical pre-treatment (n=10±SD)

3.1.3. Alloy Crystallinity and Chemistry

XRD diffraction patterns of the forged LC CoCrMo femoral stems (Figure 6) demonstrated evidence of of face centre cubic (fcc) and hexagonal close packed (hcp) crystal structures. In both cases, $(111)^{fcc}$ and $(200)^{fcc}$, $(10\bar{1}0)^{hcp}$ and $(10\bar{1}1)^{hcp}$ were observed. The relative ratios of each phase were seen to vary depending upon the processing method. For the blasted surfaces the combination of an increased ratio between the $(111)^{fcc}$ and $(1011)^{hcp}$ intensity and peak broadening relative to the polished surface could suggest a dynamic re-crystallisation and a higher degree of inhomogeneous strain within the lattice.

Fig 6 Effect of surface pre-treatment on the X-ray diffraction patterns of wrought LC CoCrMo.

FIB-TEM methods were also used in to examine the very near surface structure of the polished and blasted surfaces. Figure 7a demonstrates the light field image of the Pt-CoCrMo interface and bulk alloy with the associated areas in which diffraction analysis was conducted for the polished surfaces. A region of nano-crystalline material was visible at the top 200nm of the alloy. This is supported by dark-field images of the microstructure as shown in Figure 7b.

Fig 7 a) Light field and b) dark field TEM imaging of polished CoCrMo surfaces and SAED Patterns taken from region c) [A] and d) [B].

For added clarity Selected Area Electron Diffraction (SAED) patterns were examined at different subsurface locations. Diffraction patterns observed in the upper most regions of the surface further supported the images in Figure 7c-d, demonstrating a fine nano-crystalline layer typically characterised by the ringed diffraction pattern presented in Figure 7c. Indexing of this diffraction pattern gave a d-spacing characteristic of an hcp structure. It was also particularly interesting to see that in this case, specific points of light are visible on in the ring diffraction pattern. This further suggests that a preferential orientation along a specific crystallographic plane was seen. The diffraction pattern presented in Figure 7d suggests a single crystal with a diameter greater in length than the 300nm microscope aperture. This was indexed against a cubic structure.

Figure 8a-b demonstrates the light and dark-field images obtained for the blasted femoral stems. Changes in the subsurface microstructure were observed with the nano-crystalline material reaching depths of 400 nm; an

increase of 200nm when compared to the polished surface. Darkfield imaging again indicated finer crystallites within this region. SAED patterns were indexed as hcp cobalt in region [A] and fcc in region [B]. This is complimented by complete diffraction rings when compared to those seen in Figure 7c suggesting a finder crystallite size supporting XRD data (Figure 6). In addition to this an amorphous film ($\approx$100nm) on the blasted surfaces was observed. Point EDX analysis (Figure 8e) demonstrated this film to rich in Si and O. Traces of Cr, Co and Ca were also observed.

Fig 8 a) Light field and b) dark field imaging of a reference blasted CoCrMo surfaces and (c-d) diffraction pattern analysis of the different crystalline areas and e) TEM imagery and EDX analysis of the 100 nm Si rich film formed on the surface of the vaquasheened femoral stems.

XPS indicated a similar chemical state for Co in both the polished and blasted samples (Figure 9). Peaks were observed at binding energies of 777.98, 779.01, 781.20 and 785.10 eV suggesting the presence of metallic Co, $CoO+Co_3O_4/Co_3O_4$ and a Co^{2+} satellite respectively. A similar result was seen for the chromium surveys. Peaks were observed at 574.93, 584.01, 577.01, 586.05 eV suggesting the presence of elemental Cr and Cr_2O_3 .

Interestingly, different oxygen and carbon spectra were seen for the polished and blasted samples. Elemental oxygen (O 1s) peaks were observed around 529.25 and 532.22 eV for both polished and blasted surfaces suggesting the presence of metal oxides and H_2O respectively. An additional peak at 535.37 eV was observed on the blasted surfaces suggesting the presence of C-O/SiO_2.

Elemental C was observed in both samples at 284.25 and 284.39 eV for polished and blasted surfaces respectively. A prominent carbide (M_7C_3) peak at 283.25 eV was evident on the polished surfaces however not observed on blasted surfaces. An addition peak at 285.9 eV was seen on the blasted surfaces. This is thought to be adventitious C found on the surface. This is well known as a thin layer of carbonaceous material that is usually found on the surface of most air exposed samples. It can also be generated on the surface due to the charging nature of the surface and XPS ion etching process.

Si 2p spectra of the blasted samples further supported the TEM results (Figure 8). Resolution of the Si 2s spectra demonstrated a peak at 154.01 eV suggesting the presence of SiO_2 on the surfaces of the blasted alloy.

Fig 9 X-ray photon spectroscopy spectra for polished and blasted samples (a-b) Co 2p3/2 (c-d) Cr 2p3/2 (e-f) O 1s (g-h) C 1s. All spectra's were taken at an etch depth of 5nm and the curve fitted.

Fig 10 De-convolution of the Si 2s curves seen on blasted surfaces.

3.1.4. Static Corrosion Measurements

Potentiodynamic polarization scans were conducted on the polished and blasted surfaces to assess the relative resistance to passivity breakdown. Figure 11 shows the typical polarization curves obtained for the two surfaces using the corrected surface area calculated from measurements in section 3.1.1. Upon immersion, the E_{corr} of blasted surfaces was seen to be significantly more noble than the polished samples. After 1hr immersion E_{corr} had settled to 0.06 ± 0.02 $V_{Ag/AgCl}$ and -0.20 ± 0.03 $V_{Ag/AgCl}$ for blasted and polished samples respectively. The blasted surfaces demonstrated a lower passive current density ($I_p = 0.04\pm0.01$ $\mu A/cm^2$) compared to polished surfaces ($I_p = 2.86\pm0.15$ $\mu A/cm^2$). Breakdown of the protective oxide film and initiation of localised corrosion was seen to occur at 0.68 ± 0.05 $V_{Ag/AgCl}$ and 0.76 ± 0.08 $V_{Ag/AgCl}$ for polished and vaquasheened surface respectively. This again demonstrates that the surface subjected to blasted has an increased integrity with respect to the initiation of localised corrosion when compared to the polished surfaces.

Fig 11 Typical E vs. Log i potentiodynamic curves of polished and blasted LC CoCrMo surfaces. Surface is extrapolated from WLI measurements. Polished = 1.04 cm^2, blasted = 1.16 cm^2. Arrow indicate direction of scan.

3.2. Influence of Surface Pre-treatment on the Fretting-Corrosion Characteristics

Figure 12 demonstrates the electrochemical data collected during fretting-corrosion tests. In both cases the application of cyclic loading resulted in a shift in E_{corr} in the negative direction and increase in I_{corr}. For the blasted femoral stems, electrochemical measurements demonstrated a gradual change in E_{corr} and I_{corr} with respect to time, when compared to the polished surfaces. Upon the removal of cyclic loading, E_{corr} was seen to ennoble and a decrease in I_{corr} was seen. This signifies a partial repassivation and decrease in corrosion of the CoCrMo surfaces. Increased fretting-corrosion currents were observed for polished femoral stems when compared to the blasted femoral stems (Figure 12). After the removal of cyclic loading, corrosion currents decreased signifying a decrease in corrosion and repassivation of the metallic surfaces. Under static conditions post cyclic loading, corrosion currents were higher for the polished stem when compared to the blasted prosthesis. This was complimented by a lower corrosion potential for the polished femoral stems.

Fig 12 a) E_{corr} and b) Icorr response for femoral stems with varying surface finishes (n=3±SD).

Cumulative Faradaic mass loss (i.e. mass loss solely due to electrochemical processes) calculated from I_{corr} further supported this (Figure 13a). A linear Faradaic mass loss was seen throughout the duration of cyclic loading for polished surfaces. For the blasted system, the mass loss rates could be split into three sections. Upon the application of cyclic loading (t >24hrs) the Faradaic mass loss was seen to remain constant (similar to the rates observed under static conditions) up to 40hrs. After 40hrs, an increase in the cumulative ionic mass loss was seen until 140hrs where the rate of mass loss became constant with increasing number of cycles.

Electrochemical measurements were further supported by ICP-MS analysis of the bulk solution (Figure 13b). However the differences were not represented proportionally when compared to the Faradaic mass loss. This is due to the inclusion of additional sources of metallic debris within the bulk electrolyte.

Fig 13 Ionic mass loss a) calculated from Faraday's law and b) experimentally measured using ICP-MS (n=3±SD).

3.3. Surface Analysis of Femoral Stem and PMMA Bone Cement Surfaces

Interferometry was carried out on a select number of samples in order to quantify the extent of plastic deformation of the surface due to fretting-corrosion. Assessment of stem surface topography produced two types of data. Firstly, images of the surface were collected for each area of degradation. Secondly, surface parameters were used to quantify the degree of wear exhibited on different areas of the stem. The parameters chosen to quantify wear are shown in Table 3, along with a simple explanation of each [25].

Figure 14 demonstrates the location of the 3D interferometry analysis preformed on the polished femoral stems and counterpart PMMA bone cement after 500,000 cycles of cyclic loading. An increase in S_a was seen in the highly worn areas (SP1 and SP2) compared to distal regions of the femoral stem which were seen to be mainly affected by corrosion (SP3 and SP4) (Table 4). An increase is S_z was also seen between the areas suggesting an increased amount of plastic deformation at the proximal regions. A positive skew of the surface in SP1 indicated surface irregularities were in the positive direction. It is interesting to note that the rest of the regions were seen to exhibit a negative skew. Even though directionality of the surface in SP2 could be seen, a negative S_{sk} suggests that the extent of slip and abrasion at the interface is not as large compared to SP1. In SP3 and SP4 the negative S_{sk}, in the absence of any directionality, suggests the presence of localised pitting on the surface. This

has been confirmed by scanning electron microscopy (Figure 16-17). Pitting in the distal portions of the femoral stem was seen to range from 2-4 µm in depth.

Table 4 Measured surface parameters for polished femoral stems.

Interferometry was also conducted on the PMMA bone cement (Figure 14; CP1 and CP2). An increase in surface roughness was seen in the proximal regions of the PMMA cement, approximately 50 mm from the interface opening. Increases in surface roughness (S_a) from 0.88 to 4.52 µm were seen between bonded and debonded areas respectively due to abrasion of the PMMA cement surface.

Fig 14 Visual presentation and location of 3D interferometry analysis of polished femoral stems and counterpart PMMA bone cement after 500,000 cycles of loading.

Figure 15 and Table 5 shows the interferometry results for blasted femoral stems and the adjacent PMMA bone cement when subjected to 500,000 cycles of loading. For the blasted femoral stem, S_a and S_q were not seen to significantly differ between worn and visually unworn regions (SR1 and SR2) with analysis demonstrating similar S_a and S_q values. An increase in S_z was seen between the SR1 and SR2. In the regions were wear and corrosion had occurred (SR1), S_z along with S_{sk} measurements indicate large surface irregularities in the positive direction suggesting ploughing and plastic deformation of the surface. For surfaces that had not been affected by wear or corrosion (SR2), surface texture parameter suggested that the surface was similar to the reference stem surface. Interferometry analysis was also conducted on the counterpart PMMA cement surface. In regions where high amounts of fretting-corrosion had occurred on the femoral stem (CR1 and SR1), an increase in S_a, S_q and S_z was observed when compared to those that did not exhibited any signs of localised fretting-corrosion (CR3 and SR2).

Fig 15 Visual presentation and location of 3D interferometry analysis of blasted femoral stems and counterpart PMMA bone cement after 500,000 cycles of loading.

Table 5 Measured surface parameters for blasted femoral stems.

Figure 16 shows the surface morphology after 500,000 cycles of cyclic loading. An abrasive wear mechanism exists in and around the areas of SP1-SP2. This is present characterised by cutting of the surface (Figure 16a-b).

Towards the distal portions of the femoral stem (SP3-SP4, Figure 16c-d), where fixation remained and the level of micro-motion was low, a more localised attack of the metal surface was observed.

Fig 16 SEM SE images of polished femoral stem in areas a-b) SP1-SP2 c) SP3 and d) distal SP4.

In contrast, Figure 17 shows the surfaces of the blasted femoral stems after 500,000 cycles of cyclic loading. In the surrounding areas of SR1 (Figure 17a-b); micro-motion was present resulting in a loss of the original topography. This manifests itself in the 'polishing' effect commonly reported with blasted femoral stems. This was seen to varying degrees across the surface in the proximal portions of the femoral stems as demonstrated in Figure 17b. Toward the distal portions of the stem, the original topography remained with no indication of wear or corrosion (SR2, Figure 17c-d). In all cases where the original surface remained, PMMA debris was seen on the surface.

Fig 17 SEM SE images of blasted femoral stem in areas a) SR1 and b) SR2.

4. Discussion

Fretting corrosion of cemented femoral stems, sometimes referred to as fretting-crevice corrosion, has been highlighted in numerous clinical studies as a source of material degradation [1-3]. However the exact mechanisms and factors influencing the degradation have not been fully investigated. This study demonstrates the drastic effect surface processing has on the degradation mechanism and magnitude of corrosion found at the stem-cement interface. From the results presented in this study, surface processing is thought to affect the fretting corrosion at the stem-cement interface in two ways:

1. Modification of nano-mechanical and surface chemistry due to processing.
2. Changes to the relative micro-motion and slip mechanism present at the interface.

4.1 Effect of surface processing on surface and subsurface properties

It has been demonstrated that surface pre-treatment can have a drastic influence of the interfacial chemistry, crystalline structure and corrosion behaviour of CoCrMo alloys. XPS and TEM/EDX analysis demonstrated that mechanical pre-treatment can affect the chemistry of both the passive film and bulk material of LC CoCrMo. The formation of a SiO_2 film on the surface of the blasted stems presents an interesting finding and to the author's knowledge has not been reported before. Although the exact mechanism for the formation of such films

has not yet been elucidated, results suggest that such films are beneficial with respect to the initiation of corrosion. Blasting with aqueous glass beads increases the materials' resistance to the initiation of corrosion; however once corrosion was initiated, the vaquasheened surfaces did not have the same ability to spontaneously repassivate. This is evidenced by the higher breakdown potential, lower re-passivation potential (E_{rp}, the point at which the reverse scan crosses the forward scan) and hysteresis in the reverse loop of the polarisation plot for the blasted surface when compared to the polished surface. Such relationships have been correlated with an increase in localised corrosion across a variety of applications [26].

XPS and TEM analysis demonstrated a complex film comprising of SiO_2, Cr_2O_3 along with traces of elemental Co and Cr. It is proposed that this film results in improved corrosion characteristics, by acting as a charge transfer barrier to localised corrosion. Figure 18 schematically demonstrates the breakdown and repassivation processes of the protective Cr_2O_3 oxide layer when subjected to different surface processing techniques. It is thought that when breakdown and repassivation of the SiO_2 and Cr_2O_3 films occur, reformation of the SiO_2 will not occur resulting in a partial repassivation of the surface due to the lack of Si ion saturation at the interface. An increase in localised corrosion is thought to occur on the blasted surface due to the formation of corrosion pits capable of sustaining dissolution within the asperities on the sample surface and partial breakdown of the SiO_2 film may further lead to geometries capable of sustaining localised corrosion. It is also interesting to note the M_7C_3 carbide peak in the polished samples as seen in the XPS spectra. The loss of carbides could be beneficial when considering the application of alloys in an environment susceptible to localised corrosion [27]. Although the method of blasting used in this study is in commercial operation it must be appreciated that these results cannot be translated to grit blasting processes.

Fig 18 Schematic representation of the breakdown and repassivation of the protective Cr_2O_3 oxide layer when subjected to different surface processing techniques.

The effect of martensitic or strain induced transformations resulting in the formation of nano-crystalline material at the interface is also a factor that needs to be considered. Mechanically induced phase transformation has been shown to affect the tribological and corrosion behaviour of Metal-on-Metal (MoM) articulating surfaces [28-32]. Although CoCrMo alloys are termed austenitic, a phase change from fcc to hcp due to mechanical actions and the formation of nano-crystalline material is quite credible in these alloys. Shear transformations often result in the formation of a new lattice orientation, resulting in a new crystallographic phase and phase interfaces. The

transition between different phases is traditionally martensitic implying that no diffusion or local changes in chemistry should [33]. Mathew et al [19] has recently shown the effect of SIT on the corrosion response of CoCr supporting findings by Montero-Ocampo et al [21]. It has been shown that HC CoCr alloys possess much lower passive corrosion currents when in bulk like fcc form.

Whilst a higher degree of strain and the formation of nano-crystalline material were observed for the blasted surfaces, the effect of this transformation is unclear due to the multifactorial nature of the interface. Currently the exact role of surface reorientation is unclear. Whilst Mathew et al [19] have shown that nano-crystalline material increased corrosion currents, compressive surface processes such as blasting and shot peening are used to introduce a surface compressive stress to compact stress corrosion cracking. This work has shown that surface processes will increase the interfacial hardness of a material. However further work is needed to elucidate the effects of such films that form as a by-product of the process.

4.2 Effects of the increased surface roughness on the evolving tribocorrosion degradation mechanisms

Surface pre-treatment was also seen to influence the extent of fretting-corrosion and overall mass losses. It has been shown throughout the study that blasted surfaces demonstrated superior corrosion resistance under static and dynamic conditions. It is hypothesised that under fretting conditions, the combination of a SiO_2 film formed on the metallic surface due to the blasting process, as well as the increased interfacial strength due to interdigitation of the PMMA bone cement on the metallic surface, results in very different fretting wear and corrosion regime at the interface when compared to polished surfaces. Debonding at the stem-cement interface has been a topic of discussion for many years. Zhang et al [34] investigated the role surface roughness plays in the debonding of metallic and PMMA bone cements. Polished surfaces were seen to debond at 2.3kN, the same maximum load used in this study, whilst surfaces subjected to the same blasting process, a load of 4.0kN was required to initiate debonding. The following mechanisms for the evolving tribocorrosion degradation are proposed:

Partial and gradual debonding will occur in both cases at areas of high bending, torsional moments (i.e. proximal half of the stem). This will manifest itself within the interface as a relative micro-motion between the two surfaces, resulting in depassivation and wear enhanced corrosion of the CoCr femoral stem. For polished femoral stems, it is hypothesised that debonding and depassivation (i.e. removal of the protective oxide film) occurs immediately due to the lack of interdigitation between the PMMA bone cement with the metallic surface.

Gross slip and plastic deformation of the metallic surfaces will occur due to cement debonding, loss of local fixation and transfer of Cr_2O_3 oxides to PMMA bone cement [12]. Abrasion of the femoral stem will occur resulting in a wear-enhance corrosion as observed in the experimental data.

It is hypothesised that the blasting processes reduces corrosion at the interface through a combination of different mechanisms. The increased interfacial strength at the interface, as demonstrated by Zhang [34], will modify the slip mechanisms acting between the surfaces. The role of slip mechanisms in degradation of fretting contact is well documented in the tribology and tribocorrosion literature. Although not directly measured in this study, the shear force required to debond a metallic-cement surface will be a lot great compared to the polished surface. It is expected that a partial slip type mechanism (a combination of elastic and plastic deformation) will occur within the interface at regions where local contact conditions will be satisfied for slip and deformation to occur. This is in agreement to the findings presented by Blunt et al [35] demonstrated increased micro-motions and contact pressure to occur around micro-pores present within the cement. Due to the localised nature of the degradation process it is thought that a fatigue type mechanism will exist at asperity contacts at the cement pore-metal interface. This will result in a localised removal of material whilst other areas remain well fixed and bonded. As the fatigue processes evolve, material detachment will occur and contact conditions will be achieved allowing slip, plastic deformation and subsequent depassivation of the surface. At this point electrochemical current and potential will further shift. This can be visualised by the increase in i_{corr} with no evident depassivation between 24-60hrs (Figure 10). The increased interdigitation of bone cement with the metallic surface will also reduce the total fluid volume within the interface; reducing corrosion currents by decreasing the area available for electrochemical activity. Furthermore, areas exposed to electrolyte but subjected to insufficient micro-motion to depassivate the surface will have increased corrosion resistance due to presence of the SiO_2 film.

Whilst the corrosion currents are significantly lower for the blasted system, it must be noted that the total ionic material loss was not proportionally different. A greater amount of debris was generated by the blasted system as evidenced by ICP-MS data. This may be in the form of metallic particulates, dissolved particles and polymeric particles containing metal debris. When ionised during ICP-MS methods, all will contribute to the overall metal signal. The combination of electrochemical and ICP-MS data suggests a higher degree of abrasion exists at the blasted interface. Whilst the surface coverage of damage was not as great when compared to the

polished femoral stems, an increase in S_z suggests that the penetration of wear was greater compared to the polished stems.

Although the blasting, or vaquasheening, process improves the corrosion aspects of the system the use of such processes have been seen to have an adverse effect in the clinical application. Howie et al [36] compared similar femoral stem cohorts, of similar femoral stem geometry with the only variation of surface roughness. In all cases polished femoral stems were seen to have a superior clinical performance when compared to prosthesis with an increase surface roughness. Aseptic loosening caused by the generation of PMMA debris was given as the main driver or failure. Although not directly quantified in this study, it can be expected an increased amount of polymeric debris would be generated from the blasted stems as de-bonding progresses and would account for the higher metal content measured within the electrolyte due to the combined process of abrasion and metal transfer to the PMMA cement. Non-the-less this study has answered some of the questions posed by clinicians as to why matte stems display different wear and corrosion characteristics when compared to their polished equivalent.

Whilst this study highlights a number of important factors relating to the tribocorrosion of cemented femoral stems there are a number of limitations. Firstly due to the complex geometry and progressive nature of the degradation at the interface (i.e. subsidence etc.), the local and global contact mechanics at the interface are unknown. This is particularly important when considering the evolution of fretting corrosion currents. Whilst there is currently no quantitative solution to this, it can be seen that degradation is more localised for the blasted surfaces compared to polished surfaces. Another limitation is the lubricant adopted. Whilst this lubricant used in this study was chosen as a simplification to the system, protein containing solutions may be adopted to better understand and represent the metal-protein interactions at this interface. However it must be noted that there is still no consensus of opinion as to which lubricant best represents the synovial joint environment.

4. **Conclusions**

In conclusion, electrochemical techniques combined with visual, optical, electron microscopy and electromagnetic radiation analytical techniques have been used to quantify the influence of surface processing on the metallurgy and fretting-crevice corrosion of cemented femoral stems.

This study has demonstrated that a decrease in corrosion was seen with increasing surface roughness. Surface roughness was also seen to affect the relative contributions of wear and corrosion to the overall metallic ions

released into the bulk environment. Polished surfaces where seen to exhibit higher fretting-corrosion currents; oxidation accounted for around 60% of all metal ions released. Blasted surfaces resulted in lower wear induced corrosion; oxidation accounted for 20% of all metal ions released.

The increased corrosion resistance is due to the formation of a protective SiO_2 film formed during the blasting processing, providing a more integral barrier to corrosion. The mechanism for formation and deposition on to the surface is still unknown and subject to further investigation. Changes in the surface roughness are thought to increase interfacial strength limiting the magnitude of slip at the interface. This will decrease the levels of depassivation and subsequently reduce levels of wear enhanced corrosion.

Whilst this paper has demonstrated and proposed a mechanisms relating to the tribocorrosion of cemented femoral stems, a number of questions have arisen as a result of the findings. Questions as to how other methods of surface processing will affect the tribocorrosion processes occurring at metal-PMMA cement interfaces and the consequences of this processing on the surfaces post treatment need to be investigated.

References

1. Donell, S.T., Darrah, C., Nolan, J.F., Wimhurst, J., Toms, A., Barker, T.H.W., Case, C.P., Tucker, J.K.: Early failure of the Ultima metal-on-metal total hip replacement in the presence of normal plain radiographs. Journal of Bone & Joint Surgery, British Volume **92-B**(11), 1501-1508 (2010). doi:10.1302/0301-620x.92b11.24504
2. Hart, A.J., Quinn, P.D., Lali, F., Sampson, B., Skinner, J.A., Powell, J.J., Nolan, J., Tucker, K., Donell, S., Flanagan, A., Mosselmans, J.F.W.: Cobalt from metal-on-metal hip replacements may be the clinically relevant active agent responsible for periprosthetic tissue reactions. Acta Biomaterialia **8**(10), 3865-3873 (2013).
3. Bolland, B.J.R.F., Culliford, D.J., Langton, D.J., Millington, J.P.S., Arden, N.K., Latham, J.M.: High failure rates with a large-diameter hybrid metal-on-metal total hip replacement: clinical, radiological and retrieval analysis. Journal of Bone & Joint Surgery, British Volume **93-B**(5), 608-615 (2011). doi:10.1302/0301-620x.93b5.26309
4. Webb, J., Spencer, R.: The role of polymethylmethacrylate bone cement in modern orthopaedic surgery. The Journal of Bone and Joint Surgery **89**(B) (2007).
5. Willert, H., Broback, L., Buchhorn, G., Jemsen, P., Koster, G., Lang, I., Ochsner, P., Schenk, R.: Crevice corrosion of cemented titanium alloy stems in total hip replacements. Clin Orthop Relat Res **333**, 333-351 (1996).
6. Scheerlinck, T., Casteleyn, P.-P.: The design features of cemented femoral hip implants. Journal of Bone & Joint Surgery, British Volume **88-B**(11), 1409-1418 (2006). doi:10.1302/0301-620x.88b11.17836

7. Howell, J.R., Blunt, L.A., Doyle, C., Hooper, R.M., Lee, A.J.C., Ling, R.S.M.: In Vivo surface wear mechanisms of femoral components of cemented total hip arthroplasties: the influence of wear mechanism on clinical outcome. The Journal of Arthroplasty **19**(1), 88-101 (2004). doi:http://dx.doi.org/10.1016/S0883-5403(03)00278-X

8. Geringer, J., Forest, B., Combrade, P.: Fretting-corrosion of materials used as orthopaedic implants. Wear, 943-951 (2005).

9. Geringer, J., Macdonald, D.D.: Modeling fretting-corrosion wear of 316L SS against poly(methyl methacrylate) with the Point Defect Model: Fundamental theory, assessment, and outlook. Electrochimica Acta **79**(0), 17-30 (2012). doi:doi: 10.1016/j.electacta.2012.06.028

10. Geringer, J., Normand, B., Alemany-Dumont, C., Diemiaszonek, R.: Assessing the tribocorrosion behaviour of Cu and Al by electrochemical impedance spectroscopy. Tribology International **43**(11), 1991-1999 (2010). doi:http://dx.doi.org/10.1016/j.triboint.2010.04.018

11. Pellier, J., Geringer, J., Forest, B.: Fretting-corrosion between 316L SS and PMMA: Influence of ionic strength, protein and electrochemical conditions on material wear. Application to orthopeadic implants. Wear **271**, 1563-1571 (2011).

12. Bryant, M., Farrar, R., Brummitt, K., Freeman, R., Neville, A.: Fretting corrosion of fully cemented polished collarless tapered stems: The influence of PMMA bone cement. Wear **301**(1-2), 290-299 (2013).

13. Bryant, M., Ward, M., Farrar, R., Freeman, R., Brummitt, K., Nolan, J., Neville, A.: Failure analysis of cemented metal-on-metal total hip replacements from a single centre cohort. Wear **301**(1–2), 226-233 (2013). doi:http://dx.doi.org/10.1016/j.wear.2012.12.013

14. Geringer, J., Atmani, F., Forest, B.: Friction-corrosion of AISI 316L/bone cement and AISI 316L/PMMA contacts: ionic strength effect in tribological behaviour. Wear **267**, 763-769 (2009).

15. Bryant, M., Farrar, R., Freeman, R., Brummitt, K., Neville, A.: Fretting corrosion characteristics of polished collarless tapered stems in a simulated biological environment. Tribology International **65**(0), 105-112 (2013). doi:http://dx.doi.org/10.1016/j.triboint.2013.01.024

16. Bryant, M., Farrar, R., Brummitt, K., Freeman, R., Neville, A.: Fretting corrosion of fully cemented polished collarless tapered stems: The influence of PMMA bone cement. Wear **301**(1–2), 290-299 (2013). doi:http://dx.doi.org/10.1016/j.wear.2012.12.042

17. Bryant, M., Hu, X., Farrar, R., Brummitt, K., Freeman, R., Neville, A.: Crevice corrosion of biomedical alloys: A novel method of assessing the effects of bone cement and its chemistry. Journal of Biomedical Materials Research Part B: Applied Biomaterials **101B**(5), 792-803 (2013). doi:10.1002/jbm.b.32883

18. Bryant, M., Farrar, R., Freeman, R., Brummitt, K., Nolan, J., Neville, A.: Galvanically enhanced fretting-crevice corrosion of cemented femoral stems. Journal of the Mechanical Behavior of Biomedical Materials **40**(0), 275-286 (2014). doi:http://dx.doi.org/10.1016/j.jmbbm.2014.08.021

19. Mathew, M.T., Nagelli, C., Pourzal, R., Fischer, A., Laurent, M.P., Jacobs, J.J., Wimmer, M.A.: Tribolayer formation in a metal-on-metal (MoM) hip joint: An electrochemical investigation. Journal of the Mechanical Behavior of Biomedical Materials **29**(0), 199-212 (2014). doi:http://dx.doi.org/10.1016/j.jmbbm.2013.08.018

20. Bryant, M., Farrar, R., Freeman, R., Brummitt, K., Neville, A.: Fretting Corrosion Characteristics of Polished Collarless Tapered Stems in a Simulated Biological Environment. Tribology International (2013).

21. Montero-Ocampo, C., Juarez, R., Salinas-Rodriguez, A.: Effect of Fcc-Hcp Phase Transformation Produced by Isothermal Aging on the Corrosion Resistance of a Co-27Cr-5Mo-0.05C Alloy. METALLURGICAL AND MATERIALS TRANSACTIONS A **33** (2002).

22. I.Milosev, H.Strehblow: The composition of the surface passive film formed on CoCrMo alloy in simulated physiological solution. Electrochemica Acta **48**, 2767-2774 (2003).

23. Hodgson, A., Kurz, S., Virtanen, S., Fervel, V., Olsson, C., Mischler, S.: Passive and transpassive behaviour of CoCrMo in simulated biological solutions. Electrochemica Acta **49**, 2167-2178 (2004).

24. Fairley, N., Ltd, C.S., Ltd, C.S.: CasaXPS Manual 2.3.15: Introduction to XPS and AES. Casa Software, Limited, (2009)

25. Howell, J.R., Blunt, L., Doyle, C., Hooper, R.M., Lee, A.J., Ling, R.S.: **In Vivo Surface Wear Mechanisms of Femoral Components of Cemented Total Hip Arthroplasties**. The Journal of Arthroplasty **19**(1) (2004).

26. D.Silverman: Tutorial on Cyclic Potentiodynamic Polarization Technique. Paper presented at the Corrosion 98, 1998

27. G.Frankel: Advances in Localised Corrosion. (2011).

28. Fischer, A., Weiss, S., Wimmer, M.: The Tribologocal Difference Between Biomedical Steels and CoCrMo-alloys. Jorunal of Mechanical Behaviour of Biomedical Materials **9**, 50-62 (2012).

29. Büscher, R., Täger, G., Dudzinski, W., Gleising, B., Wimmer, M.A., Fischer, A.: Subsurface microstructure of metal-on-metal hip joints and its relationship to wear particle generation. Journal of Biomedical Materials Research Part B: Applied Biomaterials **72B**(1), 206-214 (2005). doi:10.1002/jbm.b.30132

30. Liao, Y., Hoffman, E., Wimmer, M.A., Fischer, A., Jacobs, J.J., Marks, L.D.: CoCrMo Metal-on-metal hip replacements. Phys.Chem.Chem.Phys. **15**, 746-756 (2013).

31. Liao, Y., Pourzal, R., Stemmer, P., Wimmer, M.A., Jacobs, J.J., Fischer, A., Marks, L.D.: New insights into hard phases of CoCrMo metal-on-metal hip replacements. Journal of the Mechanical Behavior of Biomedical Materials **12**(0), 39-49 (2012). doi:http://dx.doi.org/10.1016/j.jmbbm.2012.03.013

32. Pourzal, R., Theissmann, R., Morlock, M., Fischer, A.: Micro-structural alterations within different areas of articulating surfaces of a metal-on-metal hip resurfacing system. Wear **267**(5-8), 689-694 (2009).

33. Durand-Charre, M.: Microstructure of steels and cast irons. Springer, New York (1965)

34. Zhang, H., Brown, L.T., Blunt, L.A., Barrans, S.M.: Influence of femoral stem surface finish on the apparent static shear strength at the stem–cement interface. Journal of the Mechanical Behavior of Biomedical Materials **1**(1), 96-104 (2008). doi:http://dx.doi.org/10.1016/j.jmbbm.2007.06.001

35. Blunt, L.A., Zhang, H., Barrans, S.M., Jiang, X., Brown, L.T.: What results in fretting wear on polished femoral stems. Tribology International **42**(11–12), 1605-1614 (2009). doi:http://dx.doi.org/10.1016/j.triboint.2008.11.007

36. Howie, D.W., Middleton, R.G., Costi, K.: Loosening of matt and polished cemented femoral stems. Journal of Bone & Joint Surgery, British Volume **80-B**(4), 573-576 (1998).

Table 1 - Chemical composition of the Ultima TPS femoral stems tested in this study

Chemical Composition (% wt)										
C	Si	Mn	P	S	Cr	Fe	Mo	N	Ni	Co
0.05	0.19	0.67	0.005	0.0010	27.65	0.30	5.48	0.18	0.24	Bal.

Table 2 - Composition of bead blasting material used in this study

Compound	Chemical Formula	Content
Silicon Dioxide	SiO_2	73.00%
Sodium Oxide	Na_2O	15.00%
Calcium Oxide	CaO	7.00%
Magnesium Oxide	MgO	4.00%
Aluminium Oxide	Al_2O_3	1.00%

Table 3 - Surface morphology parameters [25]

Parameter	Abbreviation	Description
Average Surface Roughness	S_a	Mean height of surface topography
RMS deviation of the surface	S_q	A more 'stable' expression of surface roughness
Max. height to Min. Valley	S_z	Height between tallest peak and deepest valley
Direction of irregularities	S_{sk}	Indicates the direction of surface irregularities; zero for randomly rough surfaces, positive where peaks predominate, and negative where pits predominate

Table 4 - Obtained surface parameters for polished femoral stems.

Parameter	SP1	SP2	SP3	SP4	CP1	CP2	Reference stem surface
S_a (μm)	0.78	0.51	0.07	0.05	4.52	0.88	0.01±0.002
S_q (μm)	1.06	0.73	0.13	0.07			0.01±0.004
S_z (μm)	8.41	10.28	6.53	1.81			0.26±0.21
S_{sk}	0.92	-0.28	-2.30	-0.78			-0.30±0.23

Table 5 - Measured surface parameters for blasted femoral stems

Parameter	SR1.	SR2.	CR1.	CR2.	CR.3	Reference stem surface
S_a (μm)	0.54	0.54	0.58	0.67	0.46	0.51±0.01
S_q (μm)	0.74	0.69	0.81	0.85	0.57	0.67±0.01
S_z (μm)	9.38	7.45	12.34	10.74	7.42	7.88±0.71
S_{sk}	0.07	-0.59	-0.70	0.18	-0.17	-0.44±0.24

Figure 1
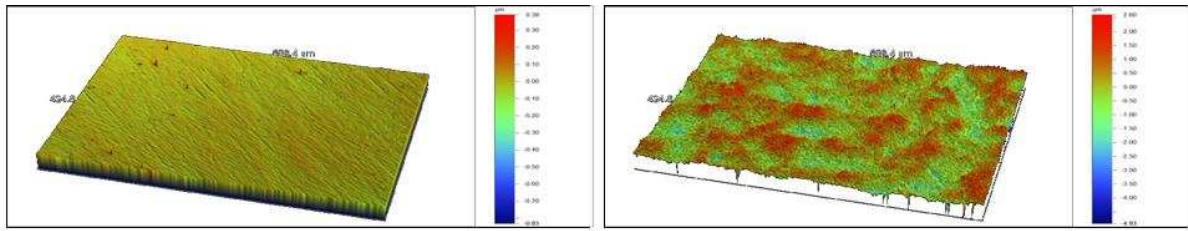
(a)   (b)
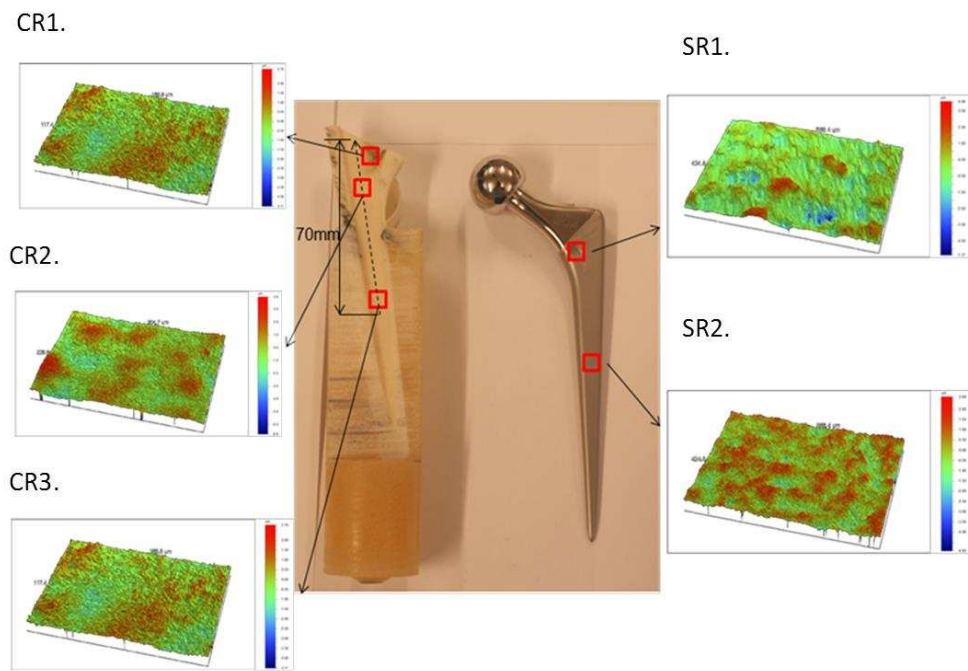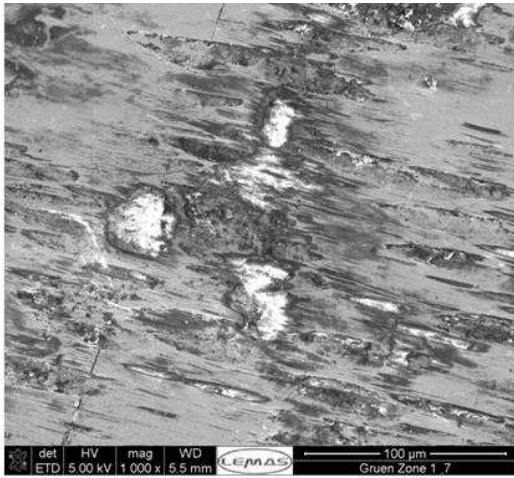
Figure 2
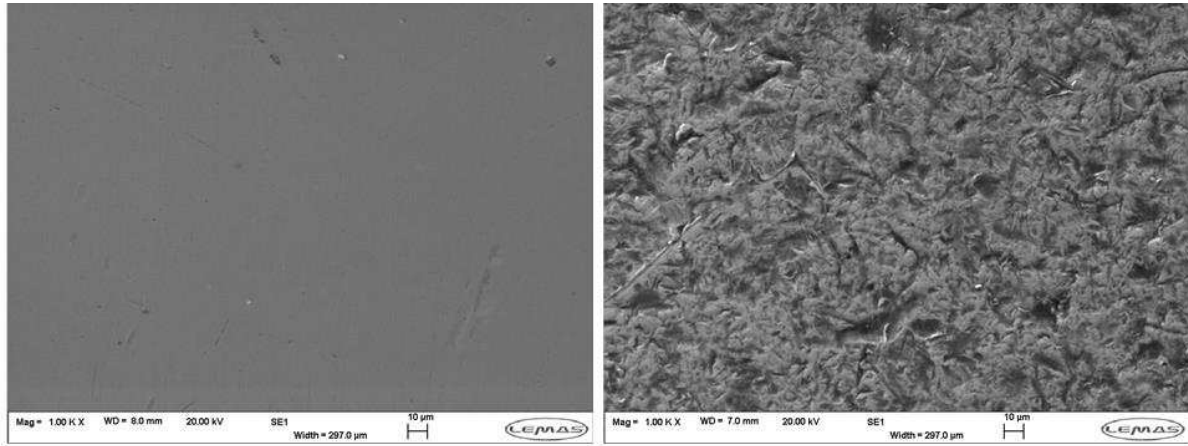
(a)   (b)

Figure 3a

(a)
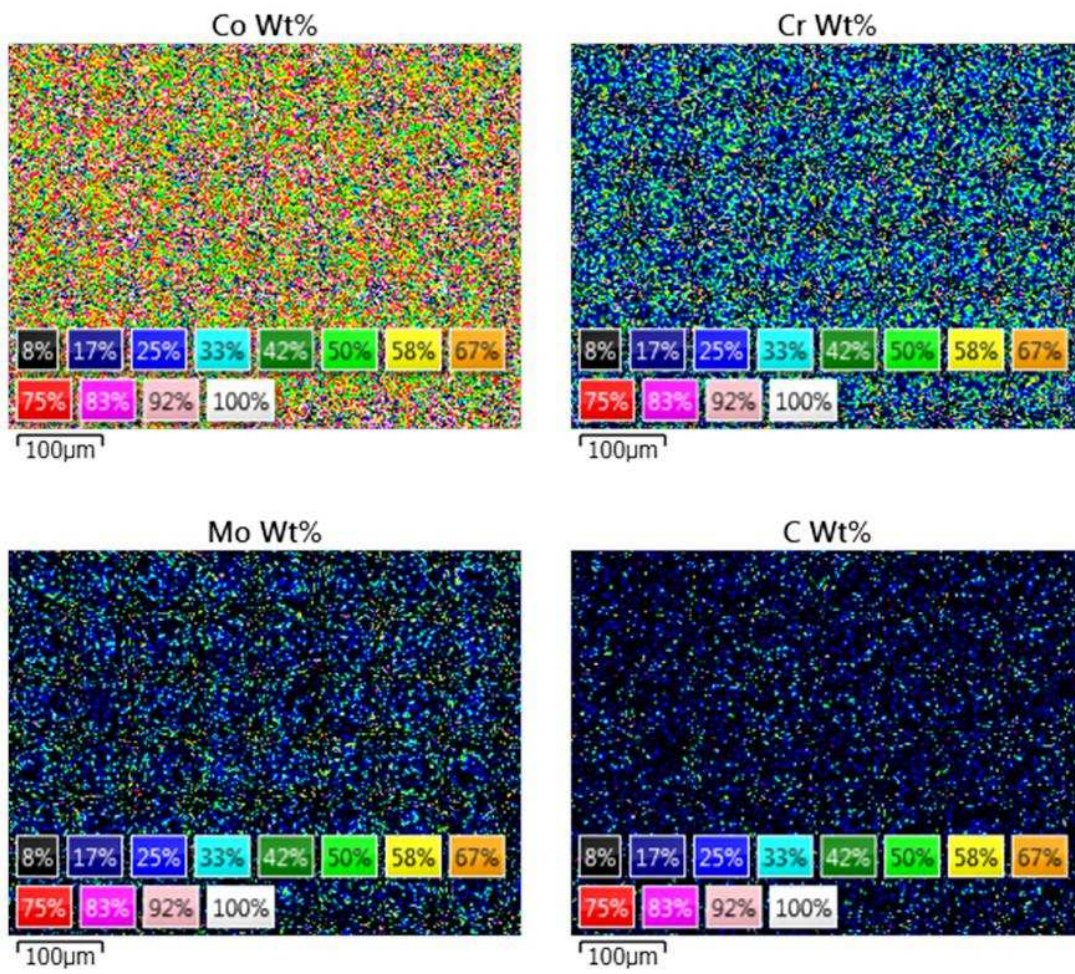
Figure 3b

(b)
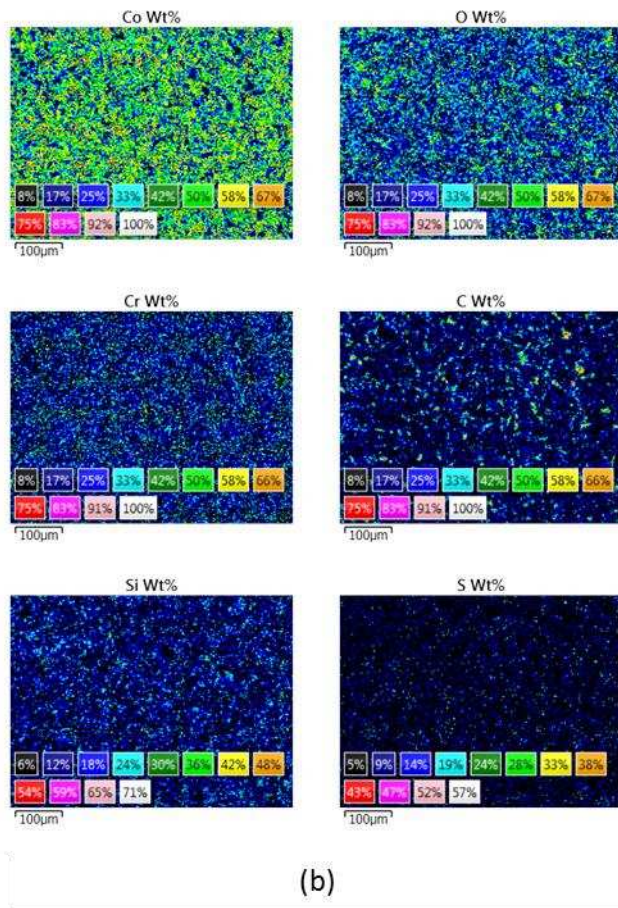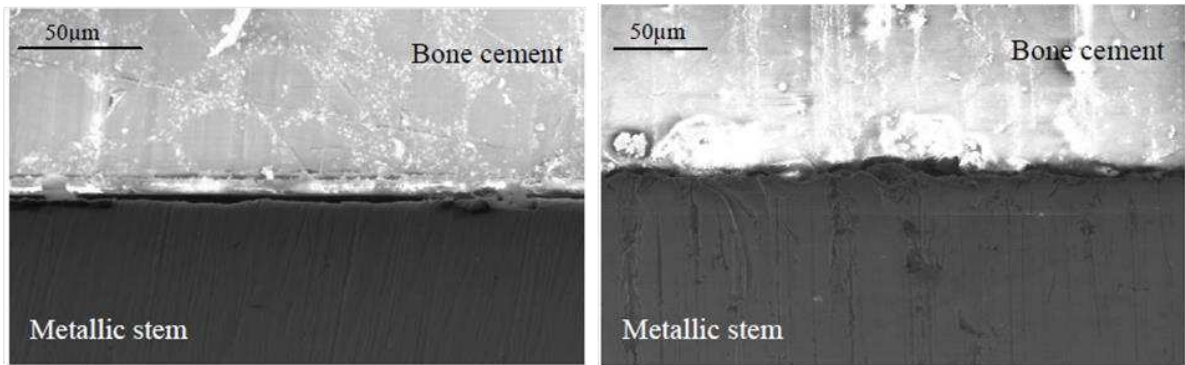
Figure 4

(a)

(b)

Figure 5
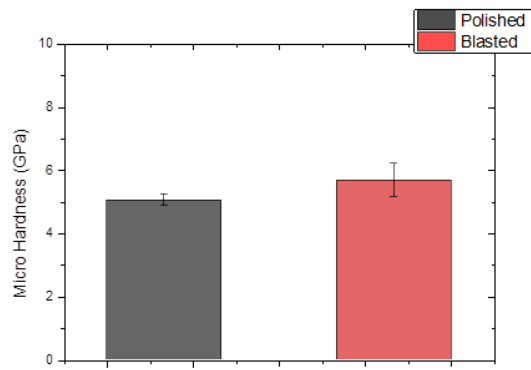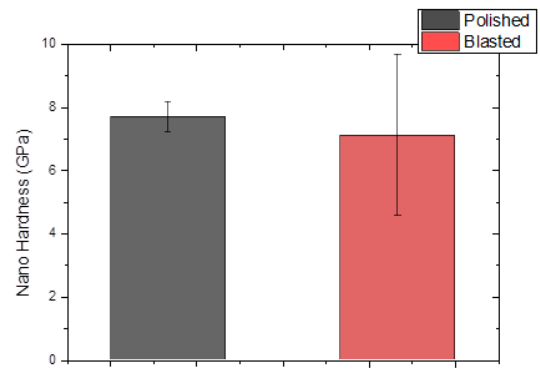
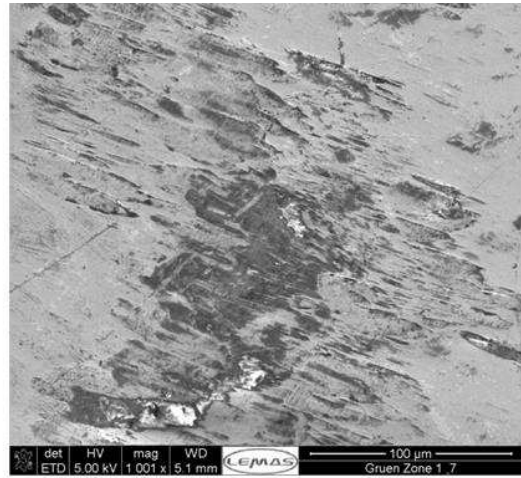

(a)   (b)

Figure 6

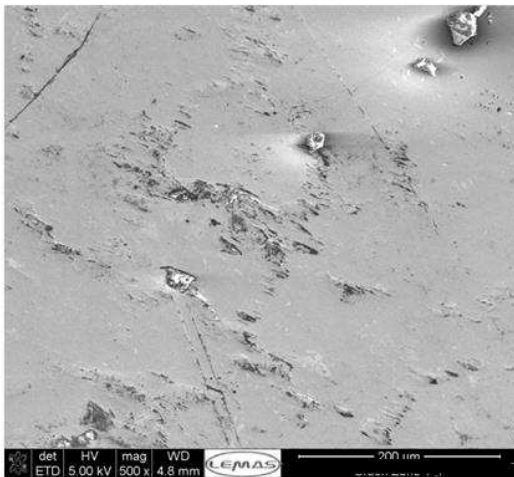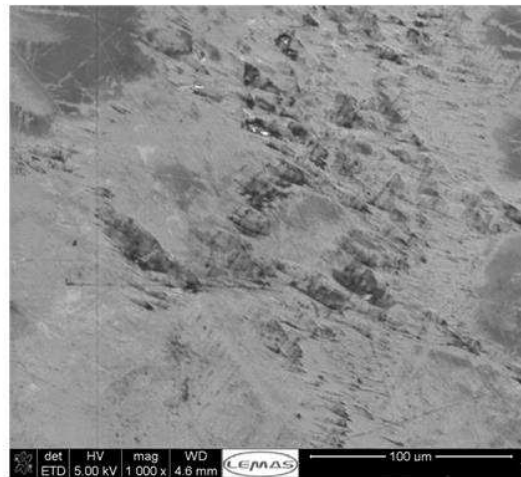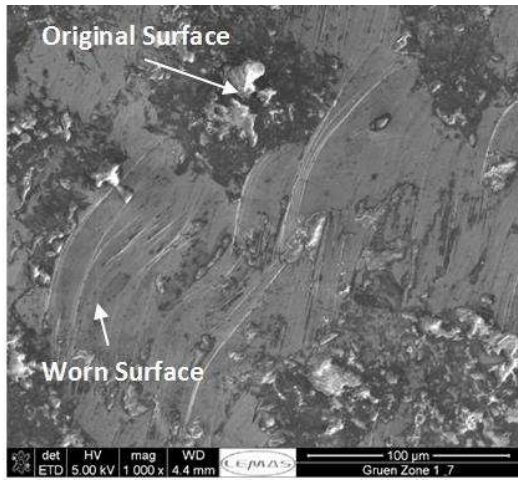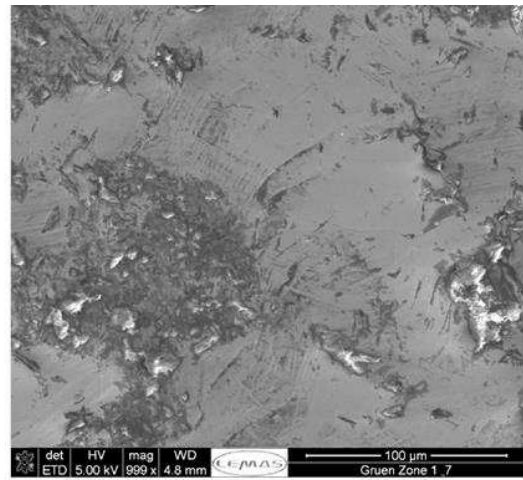Figure 7

(a)

(b)

(c)

(d)

Figure 8

(a)

(b)

(c)

(d)

(e)

Figure 9

Polished   blasted

(a)   (b)

(c)   (d)

(e)   (f)

33
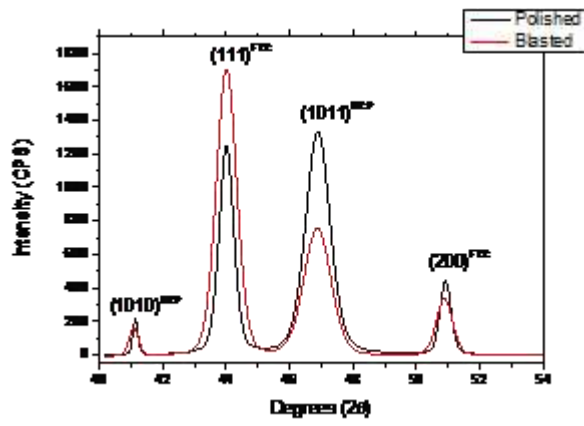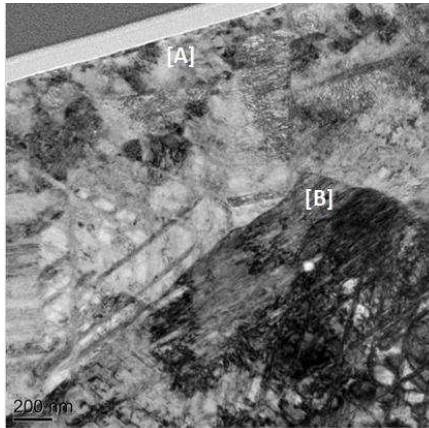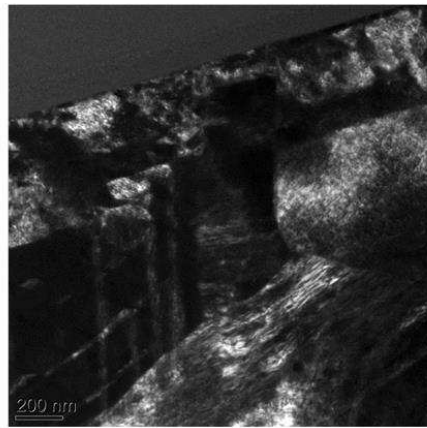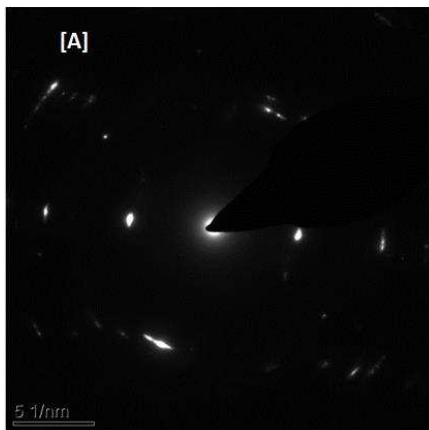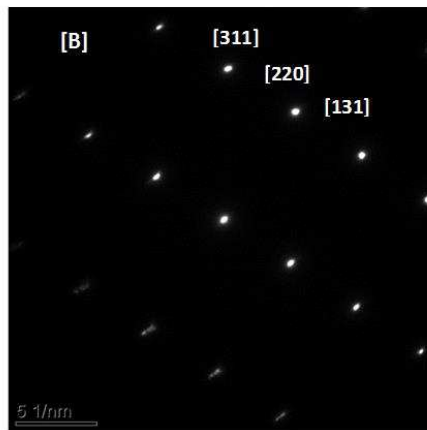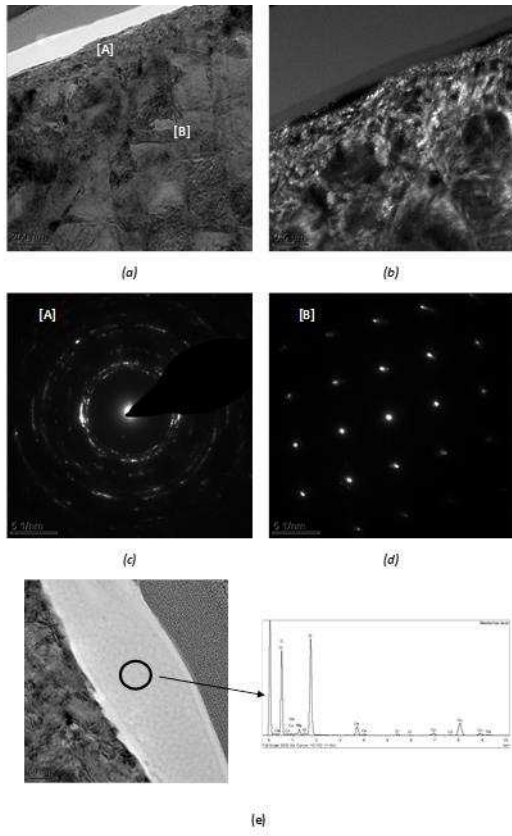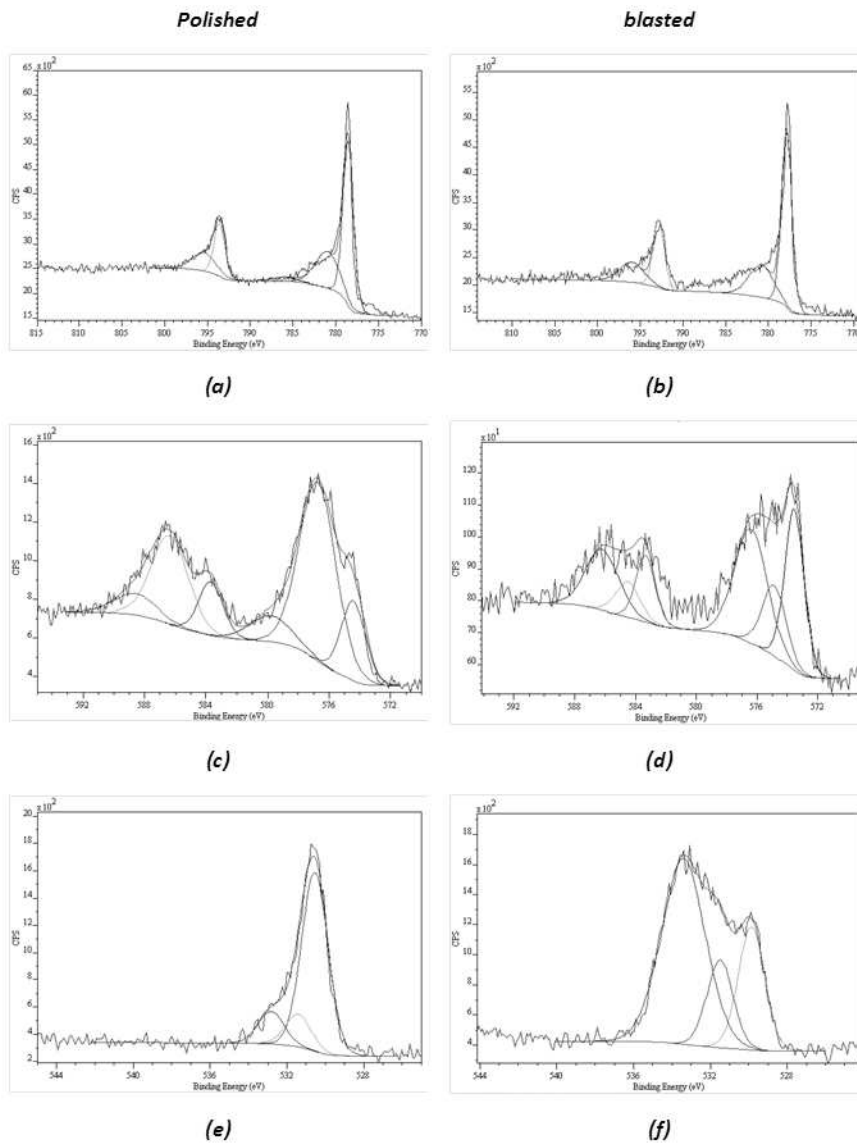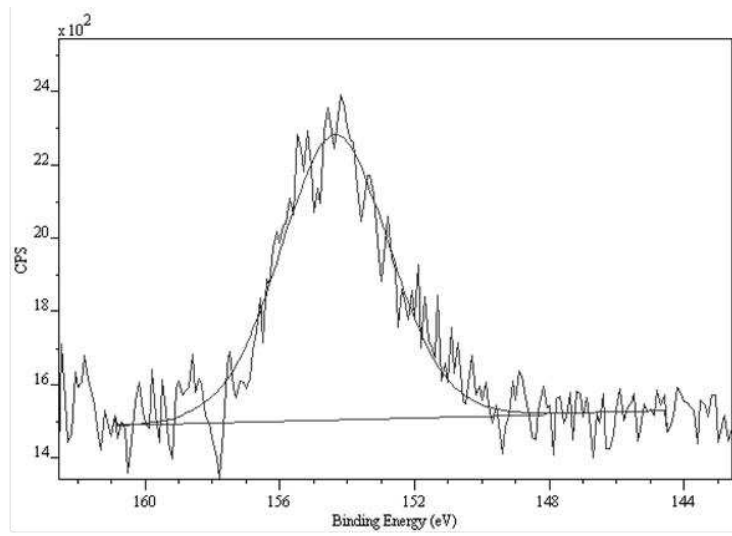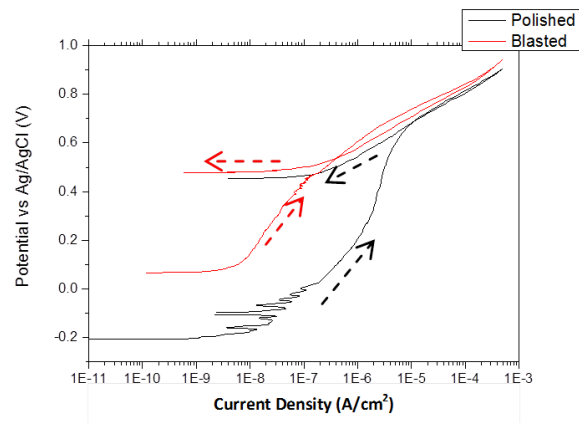
Figure 10

Figure 11

Figure 12
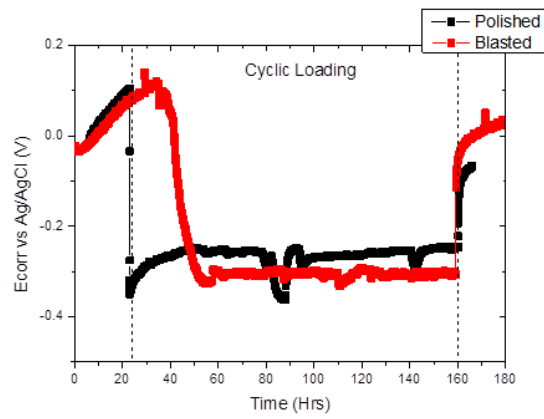
(a)
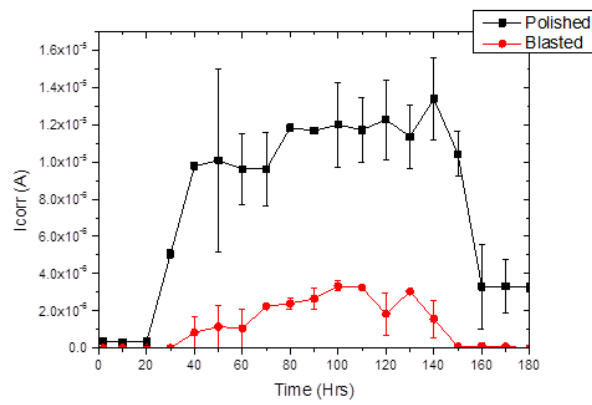
(b)

Figure 13
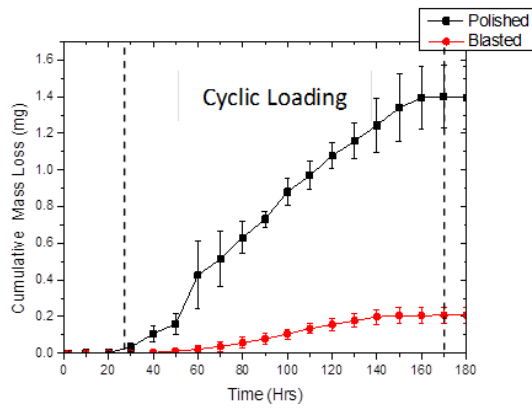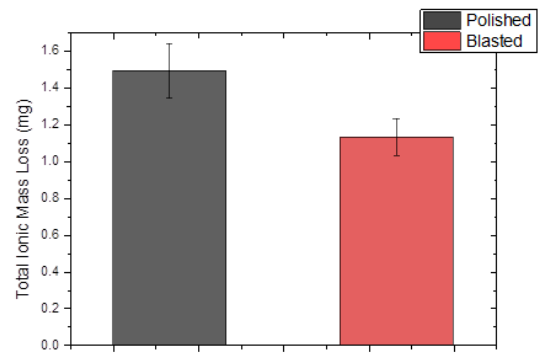
(a)   (b)

Figure 14

Figure 15

CR1.

CR2.

CR3.

SR1.

SR2.

70mm
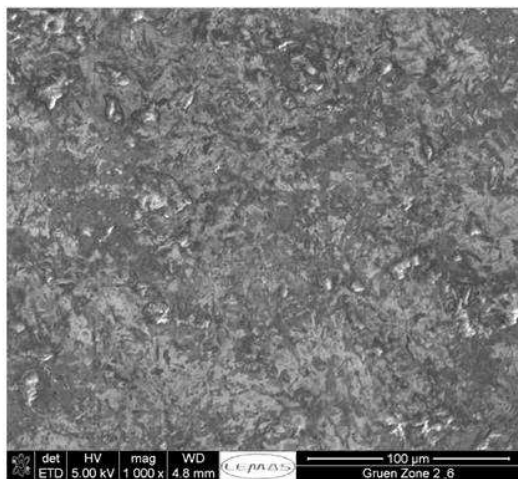
Figure 16

(a)   (b)

(c)   (d)

Figure 17

(a)

(b)

(c)

(d)